Journal of Groundwater Science and Engineering
ISSN 2305-7068
Indexed by ESCI CABI CSA
Scopus GeoRef AJ CNKI

# Potential assessment of $CO_2$ geological storage based on injection scenario simulation: A case study in eastern Junggar Basin

Xin Ma, Dong-guang Wen, Guo-dong Yang, Xu-feng Li, Yu-jie Diao, Hai-hai Dong, Wei Cao, Shu-guo Yin, Yan-mei Zhang

Citation:
Ma X, Wen DG, Yang GD, *et al*. 2021. Potential assessment of $CO_2$ geological storage based on injection scenario simulation: A case study in eastern Junggar Basin. Journal of Groundwater Science and Engineering, 9(4): 279-291.

View online: https://doi.org/10.19637/j.cnki.2305-7068.2021.04.002

Journal homepage: http://gwse.iheg.org.cn

# Potential assessment of $CO_2$ geological storage based on injection scenario simulation: A case study in eastern Junggar Basin

Xin Ma[1,2], Dong-guang Wen[1], Guo-dong Yang[3,4], Xu-feng Li[1,2*], Yu-jie Diao[1,2], Hai-hai Dong[5], Wei Cao[6], Shu-guo Yin[3], Yan-mei Zhang[7]

[1] *Center for Hydrogeology and Environmental Geology Survey, China Geological Survey, Baoding* 071051, *Hebei, China.*
[2] *Key Laboratory of Carbon Dioxide Geological Storage, China Geological Survey, Baoding* 071051, *Hebei, China.*
[3] *College of Resources and Environmental Engineering, Wuhan University of Science and Technology, Wuhan* 430081, *China.*
[4] *Hubei Key Laboratory for Efficient Utilization and Agglomeration of Metallurgic Mineral Resources, Wuhan University of Science and Technology, Wuhan* 430081, *China.*
[5] *Exploration and Development Research Institute, PetroChina Xinjiang Oilfield Company, Karamay* 834000, *China.*
[6] *Institute of Geology of Pudong Oil Production Plant, Sinopec Zhongyuan Oilfield, Puyang* 457001, *China.*
[7] *Exploration and Development Research Institute of Zhundong Oil Production Plant, Petro China Xinjiang Oilfield Company, Fukang,* 831511, *Xinjiang, China.*

**Abstract:** Carbon Capture and Storage (CCS) is one of the effective means to deal with global warming, and saline aquifer storage is considered to be the most promising storage method. Junggar Basin, located in the northern part of Xinjiang and with a large distribution area of saline aquifer, is an effective carbon storage site. Based on well logging data and 2D seismic data, a 3D heterogeneous geological model of the Cretaceous Donggou Formation reservoir near D7 well was constructed, and dynamic simulations under two scenarios of single-well injection and multi-well injection were carried out to explore the storage potential and $CO_2$ storage mechanism of deep saline aquifer with real geological conditions in this study. The results show that within 100 $km^2$ of the saline aquifer of Donggou Formation in the vicinity of D7 well, the theoretical static $CO_2$ storage is 71.967 × $10^6$ tons (P50)①, and the maximum dynamic $CO_2$ storage is 145.295 × $10^6$ tons (Case2). The heterogeneity of saline aquifer has a great influence on the spatial distribution of $CO_2$ in the reservoir. The multi-well injection scenario is conducive to the efficient utilization of reservoir space and safer for storage. Based on the results from theoretical static calculation and the dynamic simulation, the effective coefficient of $CO_2$ storage in deep saline aquifer in the eastern part of Xinjiang is recommended to be 4.9%. This study can be applied to the engineering practice of $CO_2$ sequestration in the deep saline aquifer in Xinjiang.

**Keywords:** $CO_2$ geological storage; Deep saline aquifer; Potential assessment; Injection scenarios; Numerical simulation; Junggar Basin

Received: 31 May 2021/ Accepted: 09 Oct 2021



## Introduction

The massive emission of greenhouse gases, mainly $CO_2$, has caused many environmental and ecological problems (Wang et al. 2021). Reducing $CO_2$ emission has become a common concern domestically and internationally. The experience from European and American countries and Japan shows that Carbon Capture and Storage (CCS) is one of the effective technologies to deal with global warming (Bachu, 2003; IPCC, 2005), The international community has more than ten years of practical experience in industrial scale $CO_2$ geological sequestration projects. The Sleipner and Snovit projects in the North Sea of Norway have injected nearly 20 × $10^6$ tons of $CO_2$ (GCCSI, 2016). There are a large number of sedimentary basins on both the land and continental shelf of

*Corresponding author: Xu-feng Li, *E-mail address*: lixufeng@mail.cgs.gov.cn

DOI: 10.19637/j.cnki.2305-7068.2021.04.002

Ma X, Wen DG, Yang GD, et al. 2021. Potential assessment of $CO_2$ geological storage based on injection scenario simulation: A case study in eastern Junggar Basin. Journal of Groundwater Science and Engineering, 9(4): 279-291.

Note: ① The effective storage coefficient of $CO_2$ in deep saline aquifers calculated based on the Monte Carlo model is defined as P10 when the confidence level is 90%, the effective storage coefficient of $CO_2$ is defined as P50 when the confidence level is 50%, and the effective storage coefficient of $CO_2$ is defined as P90 when the confidence level is 10%.

China, the wide distribution and extensive thickness of which provide a great potential for $CO_2$ storage (Li et al. 2006; Wen et al. 2013; Guo et al. 2015; Li et al. 2016).

Many research organizations or scholars have proposed methods for evaluating the potential of $CO_2$ geological sequestration in deep saline aquifer. Both the Carbon Sequestration Leadership Forum (CSLF) and the US Department of Energy (USDOE) have proposed standards and basic methodologies for assessing $CO_2$ sequestration capabilities (CSLF, 2005, 2007, 2010; DOE-NETL, 2006, 2008, 2010). Bachu (2003) proposed the mechanism of $CO_2$ sequestration in saline aquifer and obtained the $CO_2$ sequestration by calculating the maximum $CO_2$ dissolution of formation water (IPCC, 2005), but due to a lack of data, there would be deviation in the assessment of the storage potential of saline aquifer (Bachu et al. 2007); Goodman et al. (2011) developed a set of more specific estimation method for estimating $CO_2$ sequestration resources on regional scale based on USODE method, while Li et al. (2015), Diao et al. (2017) used GIS method in a basin-scale assessment. Some other researchers used numerical simulation, combined with field data, indoor experiment and field tests to estimate the relevant parameters based on different scenarios (Xu et al. 2010; Thomas et al. 2012; De Silva et al. 2012; Li et al. 2014; Li et al. 2015; Lee et al. 2016; Jin et al. 2017; Wen et al. 2019). Current studies on $CO_2$ saline aquifer storage are mainly based on homogeneous saline aquifers (Flett et al. 2007, Oh et al. 2013, Liu et al. 2016). Ma et al. (2018) constructed a two-dimensional heterogeneous model and randomly generated heterogeneous model to study the impact of the evaluation results on the heterogeneity potential, and there was a certain deviation between the research results and the $CO_2$ storage potential under the influence of actual heterogeneity. Sedimentary basins in China are dominated by continental sediments with complex structures, low porosity and low permeability, and their spatial distribution is generally stratified, showing strong heterogeneity. Existing studies lack the support of fine static reservoir models, so it is difficult to do a reliable potential assessment at the site scale.

The Junggar Basin is located in the northern part of Xinjiang and is the second largest inland basin in China. It is composed of 6 primary structural units, of which the Central Depression is divided into 10 secondary structural units (Fig. 1a). According to the $CO_2$ emission reduction requirements in eastern Junggar Basin and the geological conditions, China Geological Survey carried out a large number of comprehensive geological surveys of $CO_2$ storage near D7 well in the Fukang Depression in 2016 (Fig. 1b), including two-dimensional seismic survey. The survey results show that the area has a stable sedimentary environment, with good reservoir and caprock conditions, which is suitable for $CO_2$ geological storage. Based on geological survey results, this study focuses on the Junggar Basin, Xinjiang, which has great potential for CCS development in China, and takes an area of 10 km × 10 km in the eastern Junggar Basin as an example site according to the scope of seismic exploration. With well logging and two-dimensional seismic profile data, a three-dimensional heterogeneous static geological model was established. The potential of $CO_2$ geological storage was evaluated under two injection scenarios to summarize more scientific potential evaluation methods. The target reservoir is the Cretaceous Donggou Formation in the eastern Junggar Basin, with an

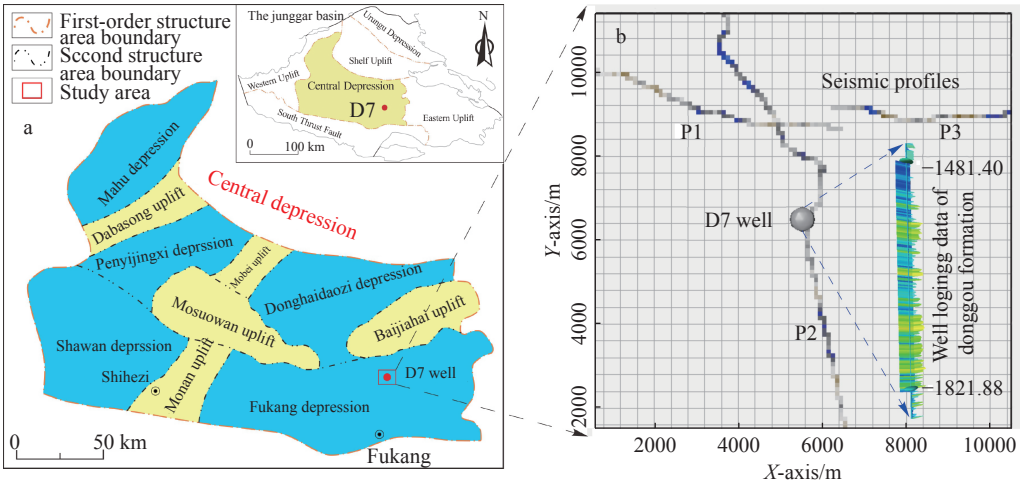


**Fig. 1** Location map of the study area and the distribution of the 2D seismic profile (Mi et al. 2018)

elevation from −1 418.40 m to −1 821.88 m and a sedimentary thickness of 340.48 m (Ma et al. 2018, Wen et al. 2019). No regional structure was developed in the study site, and the sedimentary types mainly include fine sandstone, siltstone and mudstone, and the sedimentary environment is delta-lake. The thick mudstone developed in the upper part of the Cretaceous Donggou Formation has low porosity and permeability, which can be used as a natural barrier for $CO_2$ storage by saline aquifer in the Donggou Formation.

## 1 Potential assessment approach

USDOE (DOE-NETL, 2010) method was adopted to assess the $CO_2$ storage potential:

$$G_{CO_2} = A \cdot h \cdot \varphi_e \cdot \rho_{CO_2} \cdot E_{saline} \quad (1)$$

Where: $A$ is the effective distribution area of saline aquifer, $m^2$; $h$ is the effective thickness of saline aquifer, m; $\varphi_e$ is the average effective porosity of saline aquifer; $\rho_{CO_2}$ is the $CO_2$ density under formation conditions, $kg/m^3$; $E_{saline}$ is the storage efficiency (effective factor), % （Table 1）.

**Table 1** Recommended values for $E_{saline}$ (DOE-NETL, 2010; Bachu, 2015)

| Lithology | $P_{10}$/% | $P_{50}$/% | $P_{90}$/% |
|---|---|---|---|
| Clasolite | 1.2 | 2.4 | 4.1 |
| Dolomite | 2.0 | 2.7 | 3.6 |
| Limestone | 1.3 | 2.0 | 2.8 |

## 2 Site characteristics and modelling parameters

### 2.1 Site characteristics

#### 2.1.1 Lithology

The study area is located in the Fukang Depression, the secondary structural unit of the Junggar Basin, with a stable sedimentary environment and no recent tectonic development. The target stratum mainly consists of fluvial deposit, with gentle sedimentation and a dip angle of 3°-5° slightly to the southeast, and dome structures are developed in some areas (He et al. 2002). The total thickness of the Cretaceous Donggou Formation in the eastern Junggar Basin is 356 m, which is mainly composed of mudstone, sandy mudstone with siltstone and argillaceous siltstone. According to the well logging data (D7), the elevations of the top and bottom of the Donggou Formation in the study area are −1 481.40 m and −1 821.88 m, respectively (Fig. 2). The overall permeability showed a trend of high value (maximum 441 mD) at the upper and very low at the bottom (minimum 0.001 mD) (Ma et al. 2018). The porosity had the same trend, and varied from 0.01 to 0.30 (Wen et al. 2019). At the top of the Donggou Formation, there is a layer of thick mudstone and silty mudstone (with high shale content) with a cumulative thickness of about 60 meters, which can be used as regional caprock for $CO_2$ storage in saline aquifer. Sandstone, siltstone and argillaceous siltstone (with low shale content) are interbedded with unequal thickness in the middle and lower part of the reservoir (Fig. 2). The accumulated sedimentary thickness is more than 200 meters, which can be regarded as good reservoir.

#### 2.1.2 Hydrogeology

The chemistry of the groundwater in the target layer in the study area can be described as Cl-Na type, with pH of 7.5, salinity between 35 g/L and 44 g/L (Ma et al. 2018), and chloride ion concentration between 20 g/L and 26 g/L. The water temperature is about 66℃ (Wen et al. 2019).

### 2.2 Modelling parameters

The top and bottom elevations of the Donggou Formation around the D7 well area are −1 481.40 m and −1 821.88 m respectively. According to the logging data, the temperature and pressure at the elevation of −1 540 m, in the middle of the model, are set to be 66℃ and 20.6 MPa. The pressure gradient of the formation is about 1.1 MPa /100m, and the fracture pressure of the target reservoir is about 50 MPa. The porosity is 0.010-0.296, and the permeability is 0.001 441 mD (Ma et al. 2018). For the relative permeability model of water and gas, the irreducible water saturation was set to 0.2, while the residual gas saturation set to 0.0 (Fig. 3) and the maximum residual gas saturation was set to 0.2. *Krw* is the relative permeability of the water phase; *Krg* is the relative permeability of the gas phase; *Sw* is the water saturation. Henry's law is used for modeling $CO_2$ phase behavior and solubility in the aqueous phase.

$$f_i = x_i H_i \quad (2)$$

Where: $f_i$ is the fugacity of component $i$ in the gaseous phase, $x_i$ is its mole fraction in the aqueous phase and $H_i$ is the Henry's law constant of the component.

### 2.3 Static model

The data inversion was carried out using the well logging data of D7 well and three 2D seismic

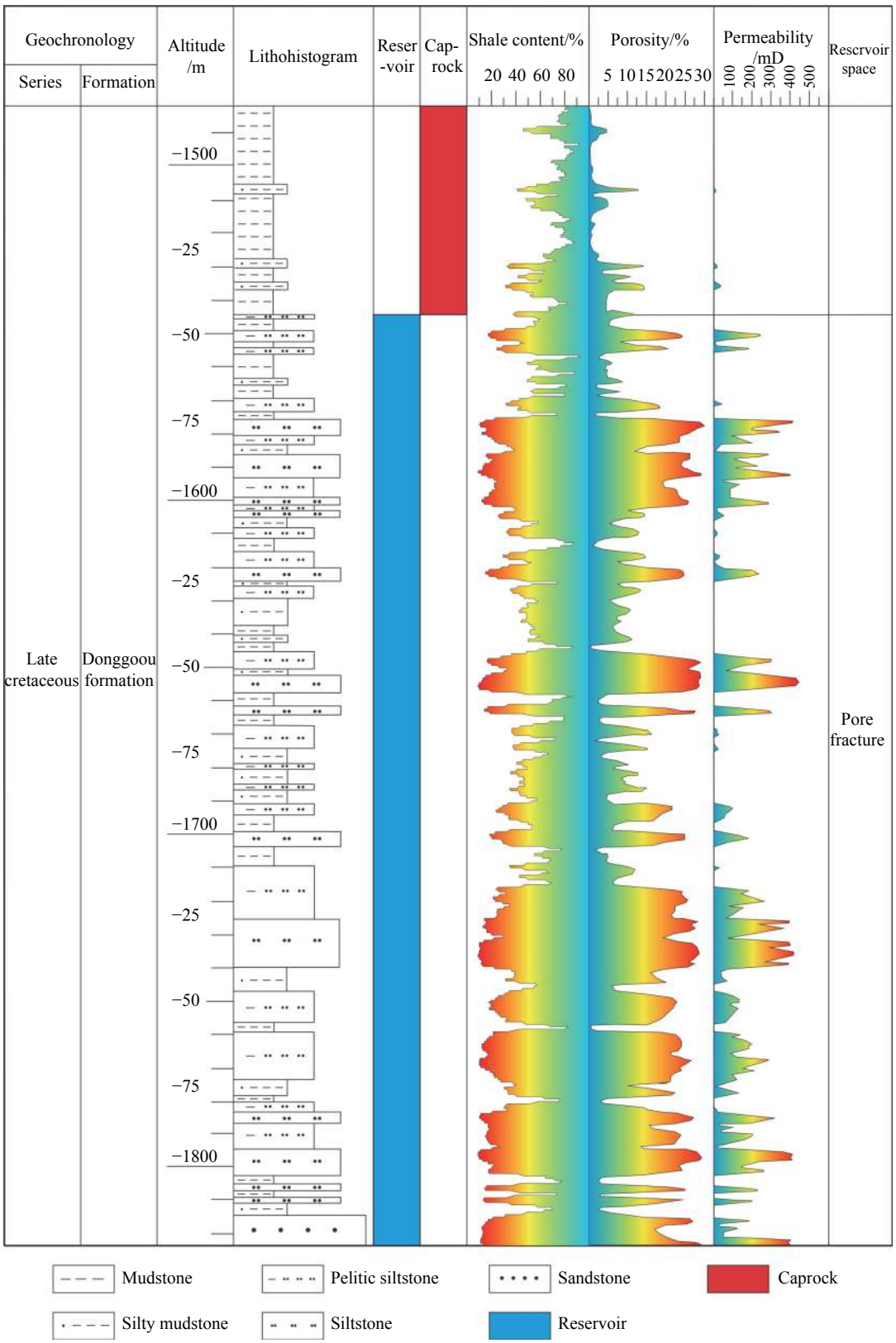


**Fig. 2** Stratigraphic histogram of Cretaceous Donggou Formation (Modified from Yang (2019))

profiles measured by China Geological Survey in 2016 (Fig. 4a). The seismic data shows that the top of the formation has a small amplitude, which indicates that the shale content is high and can be used as a regional caprock; the lower part has a large amplitude, which indicates that the shale content is low and can be used as a reservoir. The well logging data shows that mudstone is relatively well developed at the top of Donggou Formation (Fig. 4b, 4c) according to the yellow line area at the top of

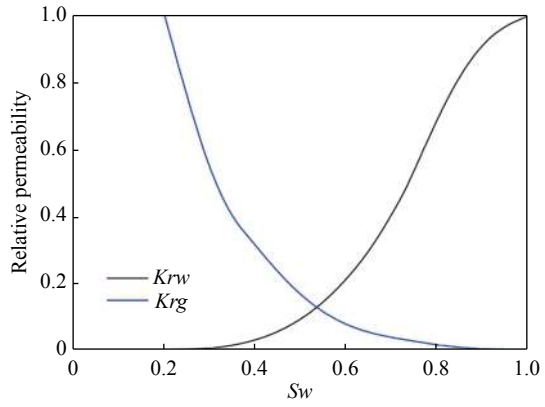


**Fig. 3** Relative permeability model for numerical simulation

the seismic profiles, and the arenaceous bodies in the middle and upper part of the formation are banded, which is consistent with the measured 2D seismic data. Through the difference fitting analysis, the fitting data were imported into the well grid, and the logging data were basically consistent with the permeability and porosity data in the grid fitting data (Fig. 4b, 4c).

According to the scope of the study area, a 10 km × 10 km static model grid was built around the D7 well, with the grid dimension of 150 m × 150 m × 5 m, and a total of 79 layers and 338 910 grid cells. Based on well logging and 2D seismic data, the permeability and porosity models of the study area were developed by using collaborative simulation method (Fig. 5). The permeabilities in X and Y directions are the same, while the permeability in Z direction is 0.3 times that in X direction (Ma et al. 2018, Wen et al. 2019).

## 3 Potential assessment results

### 3.1 Modelling scenarios

In previous studies, single-well and multi-well injections were commonly used for the dynamic potential evaluation of $CO_2$ storage in deep saline aquifers (Wen et al. 2019, Ma et al. 2018, Yang et al. 2019). In the future, million tons of $CO_2$ will be pumped into and stored in the geological formations in eastern Junggar Basin of Xinjiang to reduce $CO_2$ emission. In the actual engineering practice stage, single-well injection or multi-well group

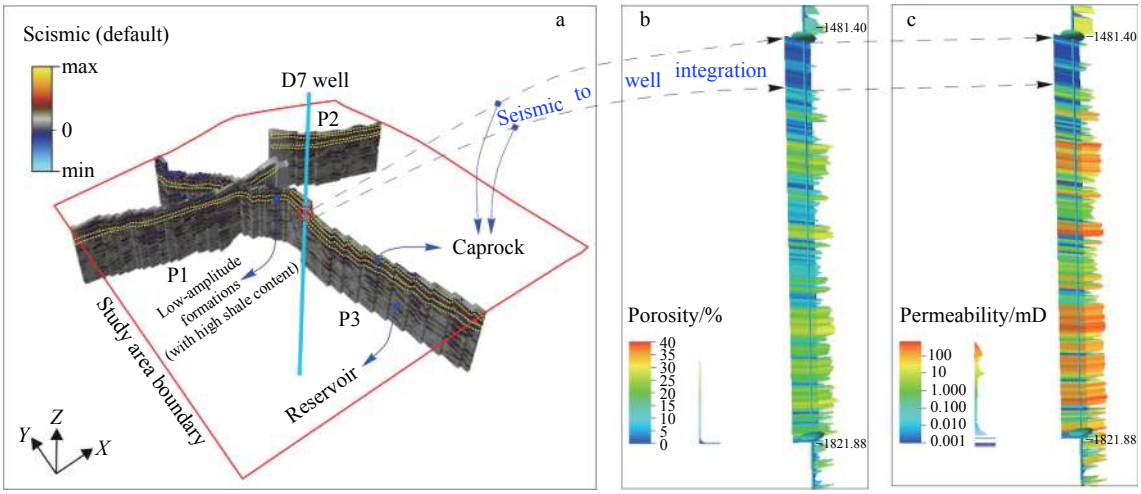


**Fig. 4** Spatial distribution of 2D seismic data and mesh data fitting of borehole

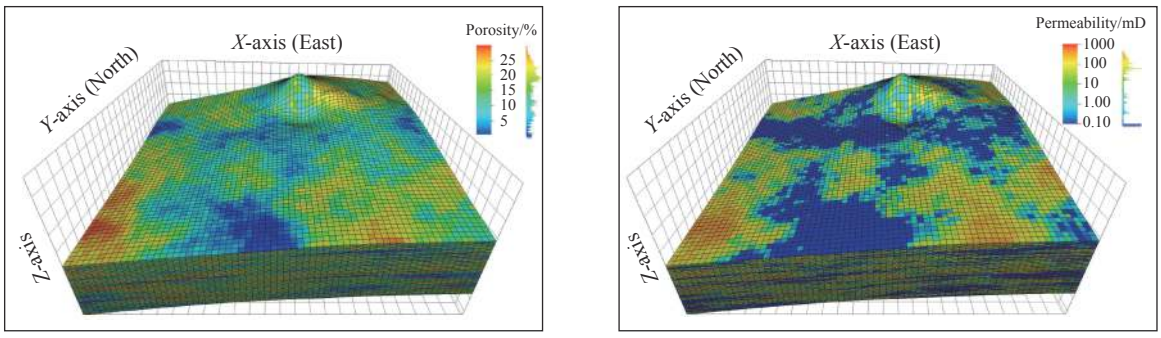


**Fig. 5** Geological models of the study area (the left is porosity model, and the right is permeability model) (Modified after Wen et al. 2019)

injection mode is generally adopted. In order to effectively support the future $CO_2$ geological storage engineering practice in eastern Junggar Basin, the scenarios of both single-well and multi-well injections are applied in this study to obtain the $CO_2$ sequestration potential and related parameters of the saline aquifer in Donggou Formation by numerical simulation (Fig. 6).

Scenario 1 (Case 1): In this case, one injection well and one production well are simulated for the duration of 300 years, to monitor whether there is leakage of $CO_2$ during the injection process. The injection well is the D7 well with the perfprated zone mainly located in the middle to lower part of the well. The injection system is unified, and the maximum allowable injection pressure at the bottom of the well is less than 50 MPa (When the injection pressure is greater than 50 MPa, the injection will be stopped). In this model, the designed $CO_2$ injection rate is $2 \times 10^6$ tons per year for 50 years, followed by 250 years of continuous simulation. The production well is set at the top of the Donggou Formation, and its maximum allowable pressure at the bottom of the well is 50 MPa.

Scenarios 2 (Case 2): In this case, five injection wells and one production well, are simulated for the duration of 300 years. The main injection well is located in the center, while the other four wells equidistantly distribute on the circumference of a circle (R = 3 km) around the D7 well. The perfprated zone is at the lower part and the injection system is unified. The same maximum allowable injection pressure is applied as in Case 1. The designed $CO_2$ injection rate is also $2 \times 10^6$ tons per year but evenly shared by 5 wells (400 000 tons/a per injection well) for 50 years, followed by 250 years of continuous simulation. The production well is set at the top of the Donggou Formation, and the maximum allowable pressure at the bottom of the well is 50 MPa.

## 3.2 Theoretical storage

The results of static modelling show that the total volume of rocks in the study area is $3.255\ 1 \times 10^{10}$ $m^3$. According to Bachu (2015), the storage efficiency is 2.4% ( $P_{50}$ ), and the sequestration of $P_{50}$ is about 71.97 million tons ( Table 2 ) (Wen et al. 2019).

## 3.3 Simulated reserve assessment

### 3.3.1 Total amount of $CO_2$ injection

In Case 1 and Case 2 models, $CO_2$ is continuously injected via injection wells at a design rate of 2 million tons per year for 50 years, with a cumulative injection amount of $1.919 \times 10^{12}$ moles (i.e. $84.41 \times 10^6$ t in total). As can be seen from Fig. 7, after $CO_2$ is injected into the reservoir, it mainly exists in two forms, namely gaseous and dissolved (aquatic) phases. The $CO_2$ contents in both gaseous

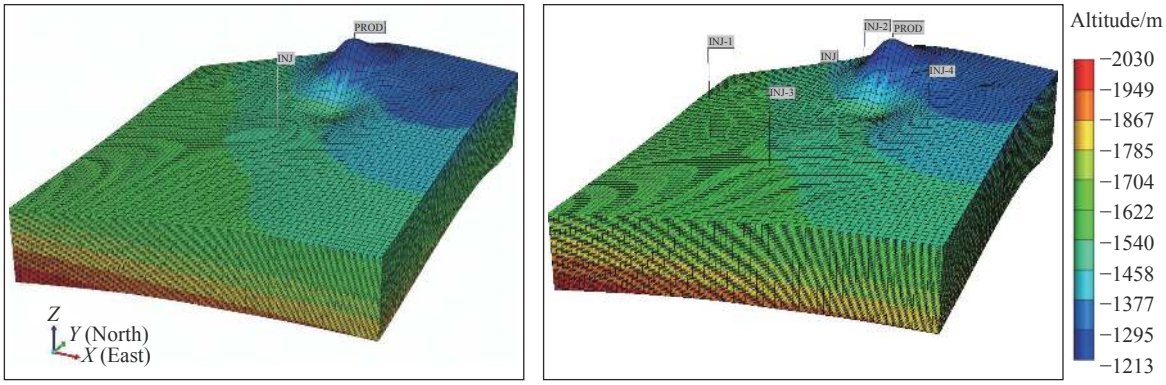


**Fig. 6** 3D geological model and well location distribution (Case 1 on the left, Case 2 on the right)

**Table 2** $CO_2$ sequestration capacity based on static modelling result

| | $P_{10}$ | $P_{50}$ | $P_{90}$ |
|---|---|---|---|
| Total volume of rocks($m^3$) | $3.255\ 1 \times 10^{10}$ | $3.255\ 1 \times 10^{10}$ | $3.255\ 1 \times 10^{10}$ |
| Storage volume ($m^3$) | $4.327 \times 10^9$ | $4.327 \times 10^9$ | $4.327 \times 10^9$ |
| Formation temperature (℃) | 66 | 66 | 66 |
| Formation pressure (MPa) | 20.6 | 20.6 | 20.6 |
| $CO_2$ density (kg/$m^3$) | 693 | 693 | 693 |
| Storage capacity (million tons) | 35.98 | 71.97 | 122.94 |

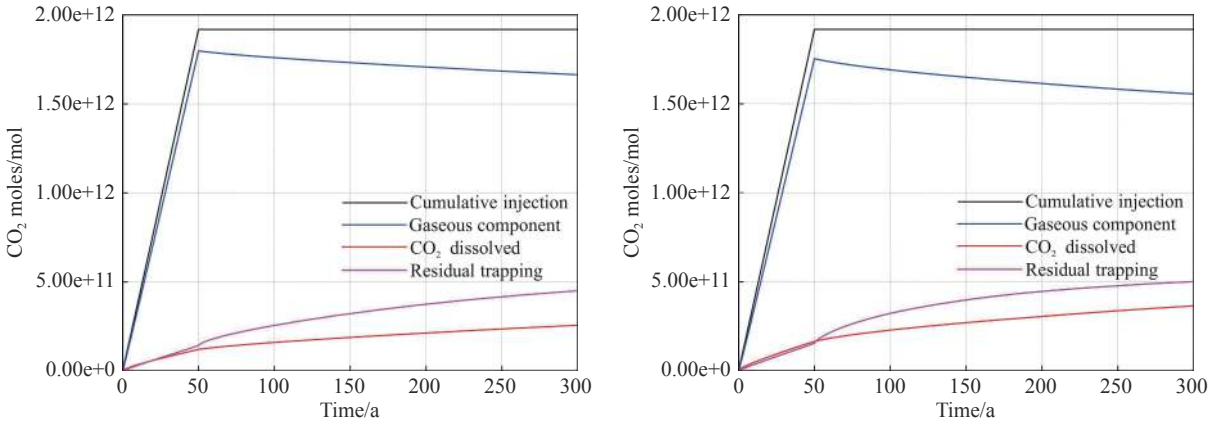


**Fig. 7** Variation of $CO_2$ in the reservoir over time (Case 1 on the left, Case 2 on the right)

and dissolved phases increase with the injection amount, of which the increase of $CO_2$ in gaseous phase is faster than that in the dissolved phase. However, after the injection is stopped, the dissolved $CO_2$ in the reservoir continues to increase while the gaseous $CO_2$ gradually decreases (Fig. 7). In the whole process of simulation, the amount of $CO_2$ captured is continuously increasing, but at the injection stage, the capture rate of $CO_2$ is always lower than the dissolution rate. After injection stops, the capture rate of $CO_2$ increases rapidly. At the end of the simulation, the total amount of $CO_2$ captured in Case 1 and Case 2 reaches $7.059 \times 10^{11}$ moles ($31.063 \times 10^6$ t in total) and $8.653 \times 10^{11}$ moles ($38.077 \times 10^6$ t in total), respectively.

The injection of $CO_2$ in the saline aquifer inevitably leads to the increase of reservoir pressure. The overall average pressures of the reservoir increased from an initial pressure of 21.878 MPa to 39.776 MPa in Case 1 and 39.615 MPa in Case 2, respectively (Fig. 8), with an increase rate of 81.81% and 81.07%. In Case 1, the pressure at the bottom of the injection well is constantly slightly greater than the average pressure of the reservoir during the injection stage. In Case 2, pressures at the bottom of INJ1 and INJ3 wells are slightly greater than the average pressure of the reservoir, which is mainly related to the depth of the injection wells. On the other hand, pressures of INJ2 and INJ4 wells at the bottom of the hole are slightly lower than the average pressure of the reservoir. Generally, the pressure of the injection well continues to increase during the injection stage, and after the completion of injection, it drops rapidly and then gradually decreases year by year. At the end of injection, the maximum increase of reservoir pressure is less than the allowed pressure of rocks, which indicates that the reservoir has good storage safety.

### 3.3.2 Spatial distribution of $CO_2$

After $CO_2$ was injected into the saline aquifer, it migrated and diffused around under the combined pressure of injection and formation. When $CO_2$ was injected into the saline aquifer, it mainly diffused upward and around the formation. Under a single well injection condition, less $CO_2$ can be sequestered at the bottom of the formation than the top, mainly because the density of $CO_2$ is much lower than that of saline water; thus under the effect of injection pressure and buoyancy, the $CO_2$ will rapidly migrate upwards, and spread along particular horizons of the formation. In the case of upward diffusion in a formation with low permeability, the vertical diffusion velocity will be very

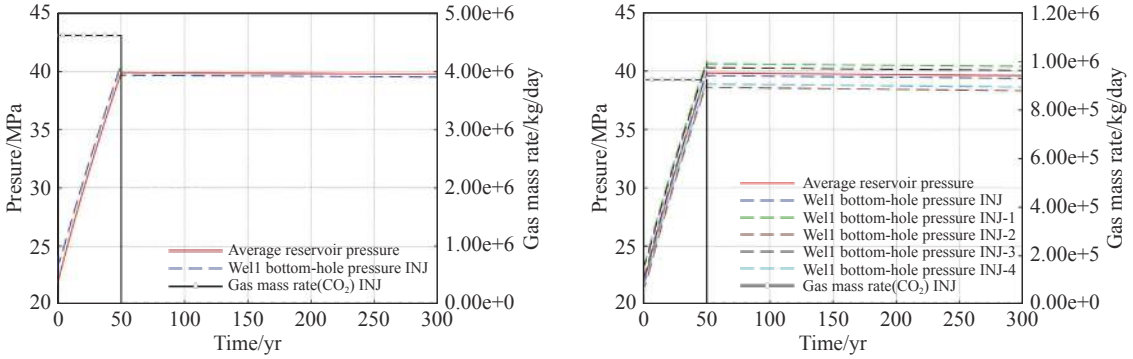


**Fig. 8** The reservoir pressure and well bottom-hole pressures over time (Case1 on the left, Case2 on the right)

limited and the horizontal diffusion will be more prominent.

As can be seen from Fig. 9, in the process of $CO_2$ storage, the gaseous $CO_2$ migrated to a maximum distance of 3 500 m in the saline aquifer during the 300 years in Case 1, and mainly migrated to the high terrain along the bedding direction of rock, while the maximum distance of vertical diffusion was about 300 m. In Case 2, the diffusion process was greatly affected by the change of the physical parameters in the formation, and the gaseous $CO_2$ preferentially entered the zones with high permeability. The $CO_2$ mainly diffused northeastwards, also in southeastern and western directions (Fig. 10). The gaseous $CO_2$ diffused around the injection well INJ to a certain distance, then migrated to the north and northeast. Similar distribution mode occurs in the INJ1 injection well in Case 2. These indicate that the difference in permeability of rock formation has a great influence on the migration path of $CO_2$. In addition, around the injection well area of INJ2, $CO_2$ did not spread around the well after entering the saline aquifer due to the influence of dome structure. It quickly entered the top of the dome structure, which indicates that the trap structure has a significant impact on $CO_2$ storage. Compared with single well injection, multi-well injection can take full advantage of reservoir space and increase the reliability of saline aquifer for $CO_2$ storage. At the same time, it was observed that $CO_2$ did not break through the argillaceous caprocks overlying the Cretaceous Donggou Formation in both Cases This suggests that the Donggou formation has a great self-storage and self-sealing ability to store $CO_2$ and is a good reservoir with a high safety factor for $CO_2$ sequestration.

Another form of $CO_2$ occurrence in the saline aquifer is the dissolved $CO_2$. Distribution of $CO_2$ is affected by temperature, pressure, salinity, permeability and other factors in the reservoir. Migration of the dissolved $CO_2$ is mainly driven by concentration difference in groundwater. In Case 1, the $CO_2$ firstly enters the saline aquifer through the upper perforated zone and then diffuses along the surface, while the dissolved $CO_2$ is mainly distributed below the middle-upper part. However, in Case 2, the dissolved $CO_2$ mainly accumulates in the middle-lower part of the reservoir due to the relatively small injection volume of each well. As soon as $CO_2$ dissolves in saline water, the density of the

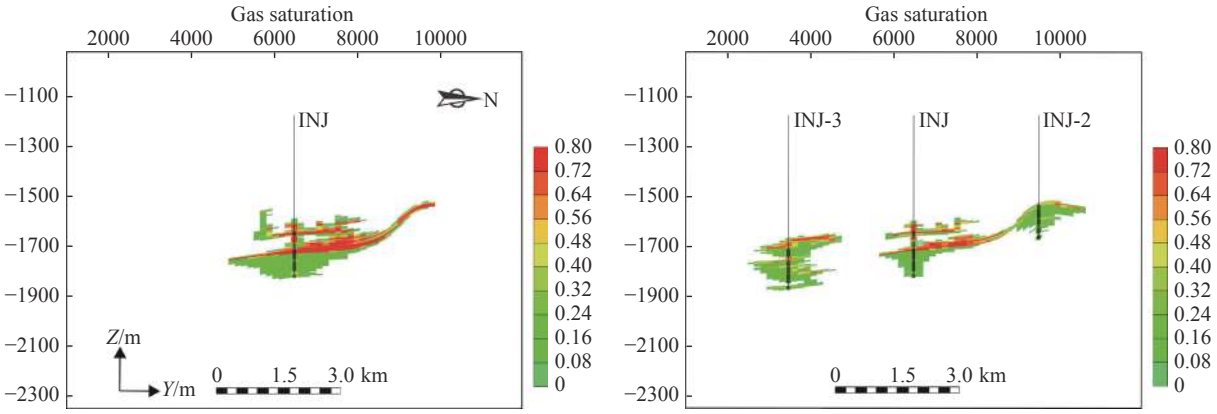


**Fig. 9** The 3D distribution of gaseous $CO_2$ at 300 years (Case1 on the left and Case2 on the right)

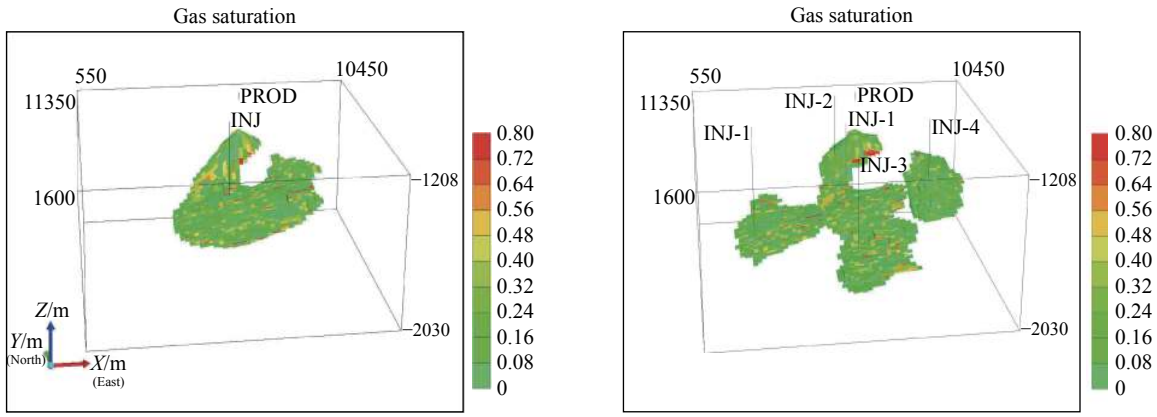


**Fig. 10** The 3D distribution of gaseous $CO_2$ at 300 years (Case1 on the left and Case2 on the right)

saline water increases and it moves downward by gravity. For example, the dissolved $CO_2$ around the INJ well almost reaches the bottom of the reservoir (Fig. 11). The distribution of the dissolved $CO_2$ near the INJ2 well is obviously affected by the trap structure. The distribution pattern of the dissolved $CO_2$ in saline aquifer is roughly the same as that of the gaseous $CO_2$, but the former has a wider extent. The dissolved $CO_2$ between the INJ and INJ2 wells is apparently connected (Fig. 11-right). In fact, dissolved $CO_2$ in the vicinity of all injection wells is well connected (Fig. 12), with the maximum north-south range of about 8.6 km, the maximum east-west range of 9.3 km and a maximum thickness of nearly 300 m.

The proportion of reservoir residual gas in Case 2 is higher than that in Case 1, mainly because the distribution area of gaseous $CO_2$ in the multiple well injection is larger than that in a single well injection (Fig. 13) to a certain extent. Therefore,

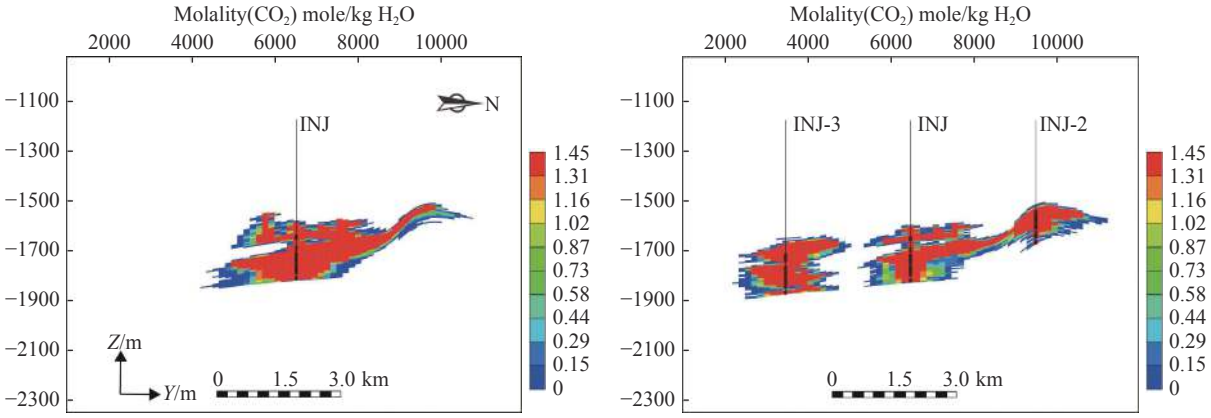


**Fig. 11** The distribution of $CO_2$ in dissolved phase in 300 years (Case1 on the left and Case2 on the right)

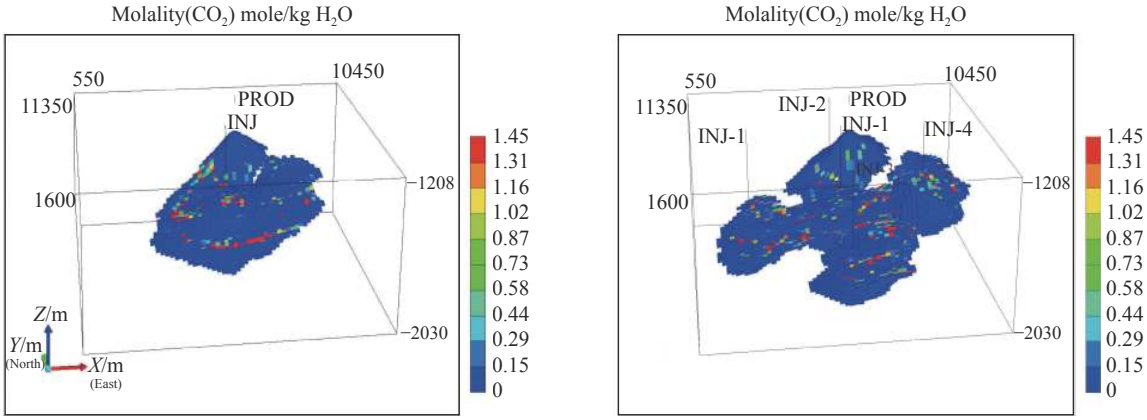


**Fig. 12** The distribution of $CO_2$ in dissolved phase at 300 years (3D) (Case1 on the left and Case2 on the right)

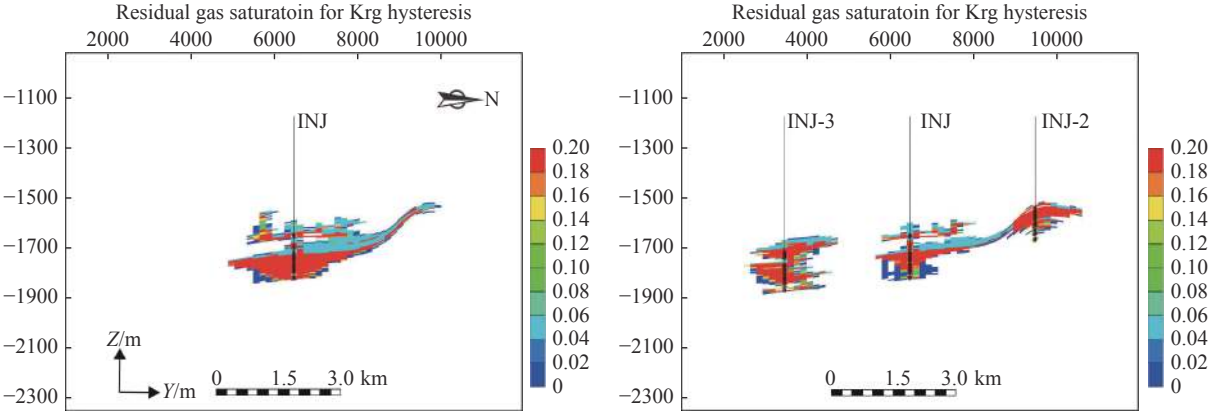


**Fig. 13** The distribution of residual trapping $CO_2$ at 300 years (Case1 on the left and Case2 on the right)

increasing the contact area between $CO_2$ and the formation rocks can lead to a higher residual gas proportion and security of $CO_2$ saline aquifer storage.

#### 3.3.3 The proportion of $CO_2$ trapping forms

From the two different injection conditions discussed above, it is estimated that a total of 84.414 million tons of $CO_2$ could be injected in 50 years. It can be seen that $CO_2$ can exists in both gaseous and dissolved phases in deep saline aquifer. However, the proportion of $CO_2$ in gas/dissolved forms is different in different injection scenarios (Table 3). Multi-well injection not only makes full use of the reservoir space, but also strengthens the hydraulic connection between the injection wells and expands the distribution of $CO_2$ in the saline aquifer. Multi-well injection is significantly better than single-well injection in terms of safety. However, from the perspective of engineering conditions, it will increase the cost to some extent. However, in Junggar Basin, where oil and gas wells are densely distributed, it is easier to apply the multi-well injection approach with a convenient operating environment.

#### 3.3.4 Influence on groundwater environment

When $CO_2$ enters the saline aquifer, the groundwater environment in the aquifer is bound to change. It will firstly increase the aquifer pressure near the injection well when the $CO_2$ enters the reservoir, and then the dissolution of $CO_2$ in the aquifer will cause reaction such as mineralization in the water and then change the density of the water body. As can be seen from Fig. 14, the density of water in the saline aquifer changes greatly after 300

**Table 3** The total amount of $CO_2$ injection and its occurrence forms

| $CO_2$ Storage Amounts in Reservoir | Case | Million tons | Percentage/% |
|---|---|---|---|
| Total injection | Case1 | 84.414 | 100.00 |
| Supercritical gas | | 73.234 | 86.76 |
| Residual trapping gas | | 19.813 | 23.47 |
| Dissolved gas in water | | 11.180 | 13.24 |
| Total trapping gas | | 31.063 | 36.71 |
| Total injection | Case 2 | 84.414 | 100.00 |
| Supercritical gas | | 68.437 | 81.07 |
| Residual trapping gas | | 22.063 | 26.14 |
| Dissolved gas in water | | 15.977 | 18.93 |
| Total trapping gas | | 38.077 | 45.07 |

Notes：The proportions of $CO_2$ in different phases to the total injection volume in the saline aquifer are given in the table. In both scenarios, the total amount of $CO_2$ injection is the same, and total trapping gas mainly consists of residual trapping gas + dissolved gas in saline water. The proportion of total trapping gas in Case 1 is 8.36% lower than that in Case 2, which is equivalent to 7.057 million tons of $CO_2$. The injection mode of Case 2 has more advantages in this regard, but the storage capacity of the two scenarios is the same.

**Table 4** Maximum dynamic storage potential of $CO_2$ in Case 1 and Case 2

| Case | Total injection/Million tons | Injection duration/yr | Storage efficiency/% |
|---|---|---|---|
| Case1 | 135.919 | 81 | 4.5 |
| Case2 | 145.295 | 95 | 4.9 |

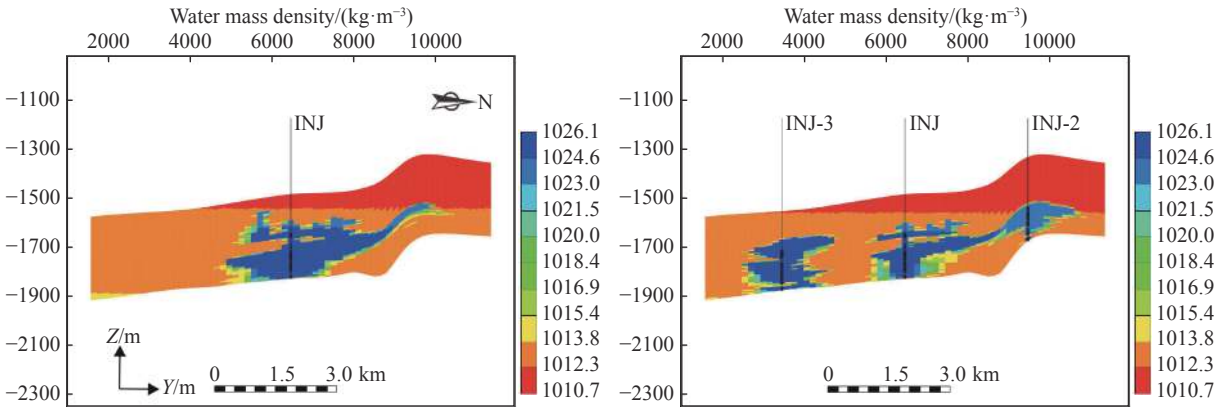


**Fig. 14** Water density distribution in the reservoir at 300 years (Case1 on the left and Case2 on the right)

years; and the closer to the injection well, the greater the variation of water density is. In the vicinity of the injection well, the density of water is increased by a maximum of 26.1‰. At the same time, when the $CO_2$ is dissolved in water, the density of water increases which results in a downward migration. The $CO_2$ is hence much safer present in dissolved phase than in the gas phase in the saline aquifers.

#### 3.3.5 Influence on reservoir pressure

When a large amount of $CO_2$ is injected into the reservoir, the reservoir pressure changes greatly. In general, the pressure in the injection well decreases radially in the surrounding area during the initial injection period. However, when the injection is stopped, the pressure gradually settles down over a period of time. After 300 years, the reservoir pressure would be leveled off. As can be seen from Fig. 15, the reservoir pressure increases from the initial maximum pressure of 24.197 MPa to 42.165 MPa and 42.007 MPa, respectively, increasing by 174.257% and 173.604%. The increase of the reservoir average pressure in Case1 is slightly higher than that in Case 2. The buried depth of the reservoir is 1 945.5 m to 2 286 m, the fracture pressure gradient of the formation is 1.63-2.25 MPa/100 m, and the maximum withstanding pressure of the rock formation is about 52.00 MPa. The maximum pressure of $CO_2$ injection into the reservoir is less than the fracture pressure of the rocks, so the reservoir has superior storability and high safety factor for the geological sequestration of $CO_2$.

After $CO_2$ is dissolved in the saline water, the density of saline water obviously increases, accompanied by a downward movement. The distribution range of the dissolved $CO_2$ in the saline water in Case 1 is obviously smaller than that of Case 2. In Case 1, the maximum migration distance of the dissolved $CO_2$ is 4 km.

#### 3.3.6 Maximum dynamic storage potential

In the above two models, $CO_2$ is continuously being injected for 50 years, and the bottom hole pressure of the injection well has not yet reached the maximum pressure that the reservoir can withstand. In order to explore the maximum $CO_2$ dynamic storage potential in this area, the injection condition of Case 1 and Case 2 models are set as: The $CO_2$ injection is stopped as soon as the bottom hole pressure of the injection well reaches 50 MPa. The $CO_2$ injection amount is regarded as the maximum dynamic storage potential of the reservoir under this condition. The simulation results show that the $CO_2$ dynamic storage potential in Case 2 is greater than that of Case 1, indicating that different injection modes may result in different storage potentials. According to the simulation result, the maximum $CO_2$ dynamic storage capacity is 145.295-$\times 10^6$ tons and the dynamic storage coefficient can reach 4.9% (Table 4). Multi-well injection can improve storage efficiency and achieve greater storage potential.

## 4 Conclusions

Based on the logging data of D7 Well and the measured 2D seismic data near the well area, a 3D heterogeneous geological model of the Cretaceous Donggou Formation was constructed on the basis of the sedimentary conditions, which reflected the distribution characteristics of the arenaceous reservoir rocks and mudstone caprock to the maximum extent, and described the distribution of porosity and permeability of the caprock. This study calculated the theoretical $CO_2$ sequestration, carried out different scenarios (Case 1 – single well injection, Case 2 – multi-well injection) through dynamic simulation, obtained the $CO_2$ sequestration of the Donggou Formation around the D7 well and the optimized dynamic simulation model, and vali-

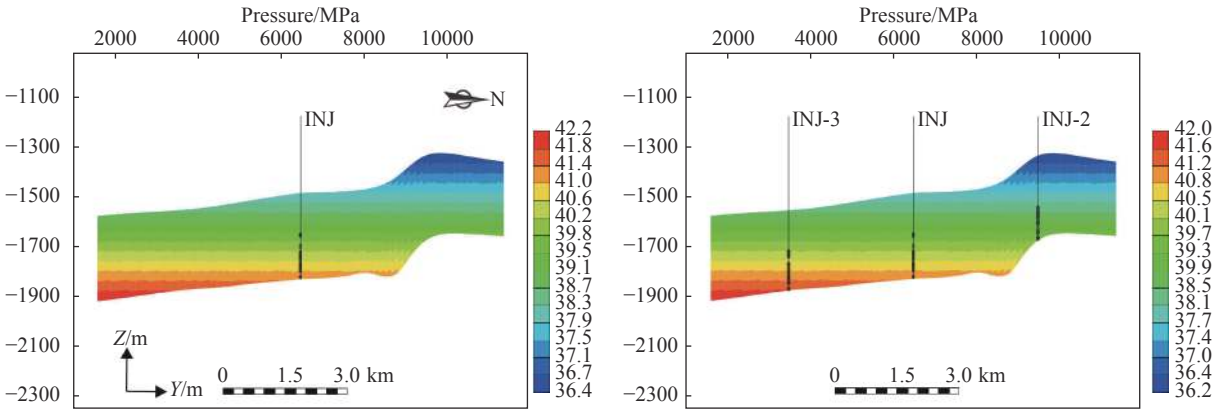


**Fig. 15** Pressure distribution in the reservoir at 300 years (Case 1 on the left side and Case 2 on the right)

dated the effective storage coefficient which is suitable for $CO_2$ sequestration in Junggar Basin. This study also revealed the $CO_2$ storage mechanism, storage potential and the $CO_2$ spatial distribution in the saline water aquifer of the Donggou Formation in the eastern Junggar Basin.

(1) The results of 3D high-reliability geological model show that the theoretical $CO_2$ storage capacity is 71.967 million tons at a guarantee rate of $P_{50}$ in the saline aquifer of Cretaceous Donggou Formation in the vicinity of the D7 well, which covers 100 $km^2$. The dynamic simulation results show that the injectable quantities of $CO_2$ in Case 1 and Case 2 are 135.919 and 145.295 million tons, respectively, while the injection duration can reach 81 years and 95 years.

(2) The $CO_2$ injected into saline aquifer mainly exists in the gaseous phase and the dissolved phase. The heterogeneity of reservoir has a great influence on the spatial distribution of the gaseous $CO_2$, such as the abrupt change of porosity and permeability, or a sudden change of terrain caused by the heterogeneous deposition, where the $CO_2$ plume is irregularly shaped or has unidirectional migration.

(3) Multi-well injection (Case 2) is more conducive to the efficient utilization of reservoir space than single well injection (Case 1), and the $CO_2$ in the dissolved phase is slightly higher. A possible explanation could be, the multi-well injection increases the contact area between the $CO_2$ and rocks, so that the proportion of residual gas is higher than that of single well injection. Also multi-well injection is safer compared with single-well injection.

(4) Based on the comparative analysis between the theoretical calculation results and the dynamic simulation results, it is suggested to set the effective coefficient $P_{50}$ as 4.9% for $CO_2$ storage capacity evaluation in the saline aquifer of Junggar Basin; and Case 2 is recommended for the dynamic calculation of $CO_2$ storage capacity.

## Acknowledgements

This work was supported by the National Natural Science Foundation of China (NSFC, Grant No. 41702284, 41602272), National key R&D program of China (Grant No. 2019YFE0100100), the Natural Science Foundation of Hubei Province, China (Grant No. 2019CFB451), and the Open Fund of Hubei Key Laboratory for Efficient Utilization and Agglomeration of Metallurgic Mineral Resources (Grant No.2020zy003). This work was also partially supported by the China Australia Geological Storage of $CO_2$ project (CAGS), and the China Geological Survey project (Grant No. DD20160307). We also would like to thank Professor Andrew Fietz and Dr. Liuqi WANG for their guidance and help while I was in Geoscience Australia.

## References

Bachu S. 2015. Review of $CO_2$ storage efficiency in deep saline aquifers. International Journal of Greenhouse Gas Control, 40: 188-202.

Bachu S, Adams JJ. 2003. Sequestration of $CO_2$ in geological media in response to climate change: Capacity of deep saline aquifers to sequester $CO_2$ in solution. Energy Conversion and Management, 44(20): 3151-3175.

Bachu S, Bonijoly D, Bradshaw J, et al. 2007. $CO_2$ storage capacity estimation: Methodology and gaps. International Journal of Greenhouse Gas Control, 1(4): 430-443.

CSLF(Carbon Sequestration Leadership Forum). 2005. "Phase I Final report from the task force for review and identification of standards for $CO_2$ storage capacity measurement, prepared by the task force on $CO_2$ storage capacity estimation for the technical group of the Carbon Sequestration Leadership Form August". Technology Report: edition 22.

CSLF(Carbon Sequestration Leadership Forum), 2007. "Estimation of $CO_2$ storage capacity in geological media (Phase), Prepared by the task force on $CO_2$ storage capacity estimation for the technical group of the Carbon Sequestration Leadership Form 15 June ". Technology Report: edition 24.

CSLF (Carbon Sequestration Leadership Forum), 2010. Task Force for Review and Identification of Standards for $CO_2$ Storage Capacity Estimation.

De Silva PNK, Ranjith PG. 2012. A study of methodologies for $CO_2$ storage capacity estimation of saline aquifers. Fuel, 93: 13-27.

Diao YJ, Zhu GW, Cao H, et al. 2017. Mesoscale assessment of $CO_2$ storage potential and geological suitability for target area selection in the Sichuan Basin. Geofluids, 2017(1): 1-17.

DOE-NETL. 2006. Carbon Sequestration Atlas of the United States and Canada.

DOE-NETL. 2008. Carbon Sequestration Atlas of the United States and Canada, 2nd edition.

DOE-NETL. 2010. Carbon Sequestration Atlas of the United State and Canada, 3rd edition.

Flett M, Gurton R, Weir G. 2007. Heterogeneous saline formations for carbon dioxide disposal: Impact of varying heterogeneity on contain-

ment and trapping. Journal of Petroleum Science and Engineering, 57(1-2): 106-118.

GCCSI. THE GLOBAL STATUS OF CCS. 2016. Available on https://www.globalccsinstitute.com/ resources/publications-reports-research/the-global-status-of-ccs-2016-summary-report/.

Goodman A, Hakala A, Bromhal G, et al. 2011. US DOE methodology for the development of geologic storage potential for carbon dioxide at the national and regional scale. International Journal of Greenhouse Gas Control, 5(4): 952-965.

Guo JQ, Wen DG, Zhang SQ, et al. 2015. Potential and suitability evaluation of $CO_2$ geological storage in major sedimentary basins of China. Acta Geological Sinica (English Edition), 89(4): 1319-1332.

He K, Zhu YS, Wang Z, et al. 2002. The Reservoir -Forming Conditions and Analyses of CretaceousExploration Prospect in the East of Junggar Basin. Journal of Xinjiang Petroleum Institute, 14(2): 6-9, 80. (in Chinese)

IPCC. 2005. Special Report on Carbon Dioxide Capture and Storage.

Jin C, Liu LT, Li YM, et al. Capacity assessment of $CO_2$ storage in deep saline aquifers by mineral trapping and the implications for Songliao Basin, Northeast China. Energy Science & Engineering, 2017, 5(2): 81-89.

Lee H, Seo J, Lee Y, et al. 2016. Regional $CO_2$ solubility trapping potential of a deep saline aquifer in Pohang basin, Korea. Geosciences Journal, 20(4): 561-568.

Li PC, Zhou D, Zhang CM, et al. 2015. Assessment of the effective $CO_2$, storage capacity in the Beibuwan Basin, offshore of southwestern PR China. International Journal of Greenhouse Gas Control, 37: 325-339.

Li Q, Chen ZA, Zhang JT, et al. 2016. Positioning and revision of CCUS technology development in China. International Journal of Greenhouse Gas Control, 46: 282-293.

Li Q, Wei YN, Liu G, et al. 2015. $CO_2$-EWR: A cleaner solution for coal chemical industry in China. Journal of Cleaner Production, 103: 330-337.

Li Q, Wei YN, Liu GZ, et al. 2014. Combination of $CO_2$ geological storage with deep saline water recovery in western China: Insights from numerical analyses. Applied Energy, 116: 101-110.

Li XC, Liu YF, Bai BF, et al. 2006. Ranking and screening of $CO_2$ saline aquifer storage zones in China. Chinese Journal of Rock Mechanics and Engineering, 25(5): 963-968. (in Chinese)

Liu DQ, Li YL, Song SY, et al. 2016. Simulation and analysis of lithology heterogeneity on $CO_2$ geological sequestration in deep saline aquifer: A case study of the Ordos Basin. Environmental Earth Sciences, 75(11): 1-13.

Ma X, Li XF, Yang GD, et al. 2018. Study on Field-scale of $CO_2$ Geological Storage Combined with Saline Water Recovery: A Case Study of East Junggar Basin of Xinjiang. Energy Procedia, 154: 36-41.

Mi ZX, Wang FG, Yang YZ, et al. 2018. Evaluation of the potentiality and suitability for $CO_2$ geological storage in the Junggar Basin, northwestern China. International Journal of Greenhouse Gas Control. 78: 62-72.

Oh J, Kim K Y, Han WS, et al. 2013. Experimental and numerical study on supercritical $CO_2$/brine transport in a fractured rock: Implications of mass transfer, capillary pressure and storage capacity. Advances in Water Resources, 62(12): 442-453.

Thomas MW, Stewart M, Trotz M, et al. 2012. Geochemical modeling of $CO_2$, sequestration in deep, saline, dolomitic-limestone aquifers: Critical evaluation of thermodynamic submodels. Chemical Geology, 306-307: 29-39.

Wang Y, Guo CH, Zhuang SR , et al. 2021. Major contribution to carbon neutrality by China's geosciences and geological technologies. China Geology, 4: 329-352.

Wen DG, Ma X, Wang LQ, et al. 2019. Combined study of static and dynamic reservoir modelling for the $CO_2$ storage project in deep saline aquifer in Zhundong, Xinjiang, China. In 14th Greenhouse Gas Control Technologies Conference Melbourne 21-26 October 2018 (GHGT-14). Melbourne. Social Science Electronic Publishing. https://doi.org/10.2139/ssrn.3365930

Wen DG, Guo JQ, Jia XF, et al. 2013. The progress of carbon dioxide geological storage research and pilot project in China. Acta Geologica Sinica, 87: 971. (in Chinese)

Xu TF, Kharaka YK, Doughty C, et al. 2010. Reactive transport modeling to study changes in water chemistry induced by $CO_2$ injection at the Frio-I Brine Pilot. Chemical Geology, 271: 153-164.

Yang ZJ, Xu TF, Wang FG, et al. 2019. A study on the $CO_2$-Enhanced water recovery efficiency and reservoir pressure control strategies. Geofluids: 1-17.